ACTIVE PULSE STRUCTURAL CONTROL USING ARTIFICIAL NEURAL NETWORKS

By Shih-Lin Hung,[1] C. Y. Kao,[2] and J. C. Lee[3]

ABSTRACT: Increasing interest has focused on applying active control systems to civil engineering structures subjected to dynamic loading. This study presents an active pulse control algorithm, termed the adaptive neural structural active pulse (ANSAP) controller, to control civil engineering structures under dynamic loading. The ANSAP controller minimizes structural cumulative responses during earthquakes by applying active pulse control forces. The effect of pulses is assumed to be delayed until just before the next sampling time so that the control force can be calculated in time and applied; the newly developed control strategy circumvents the effect of time delay due to the computation time. The ANSAP controller also circumvents the difficulty of obtaining system parameters of a real structure for the algorithm for active structural control. Illustrative examples reveal significant reductions in cumulative structural responses, which demonstrates the feasibility of using the adaptive artificial network for controlling civil engineering structures under dynamic loading.

INTRODUCTION

The control of civil engineering structures subjected to dynamic loadings, such as those attributed to earthquakes, heavy winds, and high waves, can be classified into passive and active controls. A passive control system does not require an external power source. On the other hand, an active control system is one in which an external source powers one or more control actuators that apply forces to the structure in a prescribed manner. Active control devices are used in civil engineering structures to modify the structural parameters (stiffness and damping), allowing them to more favorably respond to the external excitation (Soong 1990). Passive and active control largely differ in that the former does not make any real-time changes in the system.

Recent advances in the use of active control devices in civil engineering structures have been achieved not only in the control algorithms used but also in the experimental studies of laboratory scale-model and full-scale structures (Chung et al. 1988; Reinhorn et al. 1993). Among the several control algorithms used for active control of civil engineering structures are standard optimal control, instantaneous optimal control, pole assignment, and pulse control (Masri et al. 1981; Udwadia and Tabaie 1981a,b; Pantelides and Nelson 1995).

Standard optimal control requires the entire time history of a structural response to compute the necessary external applied force. Hence, optimization in the standard optimal control approach aims to minimize the objective function in the global sense. Another approach, an instantaneous optimal control algorithm (Yang et al. 1987), has been developed to achieve online control for civil engineering structures. In this approach, optimization is achieved only within each small time interval rather than globally. The pole assignment control algorithm has been extensively studied in control literature (Sage and White 1977). Its applications to the study of civil engineering structural control have been fruitful only when a few vibration modes contribute significantly to the response. Udwadia and Tabaie (1981b) developed an optimal pulse control algorithm for a linear system. It is heuristic in nature and requires continuous monitoring of the system state; when the system response exceeds some specified threshold, an open loop pulse control is applied at a set of preassigned actuator locations.

Despite their many attractive features, conventional control techniques may encounter difficulties when controlling systems that are difficult to model. Besides, complex conventional control laws increase the computational time in the loop, resulting in poor control. Housner et al. (1994) indicated that the control strategies deemed appropriate for civil engineering structural control should be simple, but robust and fault tolerant; in addition, they do not need to be optimal controls, and they must be implemented. Notably, the artificial neural network (ANN) model is robust and fault tolerant (Rumelhart et al. 1986; Adeli and Hung 1995; Johan et al. 1996). In addition, ANN can effectively deal with qualitative, uncertain, and incomplete information. Therefore, ANN is highly promising for active structural control.

Nikzad and Ghaboussi (1991) first applied multilayered feedforward networks (MFN) to the problem of digital vibration control of mechanical systems. The comparison between conventional control and the controller using a trained MFN clearly shows the superior performance of the neural network control. Wen et al. (1992) used two ANNs: one to predict the structural response subjected to the control force alone, and the other to predict ground accelerations. That same investigation introduced the concept of a time delay since the control force was applied at the next time step. Tang (1995) proposed a simple heuristic-based control strategy capable of applying the control force to cancel the system velocity at the preceding time step for a single-degree-of-freedom system. The underlying notion of the heuristic-based control strategy is pulse control (Udwadia and Tabaie 1981a).

In light of the above developments, this work presents a novel ANN active pulse control model, the adaptive neural structural active pulse (ANSAP) controller, to control civil engineering structures under dynamic loadings. The proposed model is based on an artificial neural network active control model with a pulse control strategy. Instead of using a standard back-propagation (BP) ANN learning algorithm, the proposed ANN active control model uses a more effective limited memory Broyden-Fletcher-Goldfarb-Shanno (L-BFGS) ANN learning algorithm (Hung and Lin 1994) with a modified BP ANN learning algorithm. The proposed control strategy attempts to reduce the structural cumulative responses during earthquakes by applying the active pulse control force. The ANSAP controller has two components: (1) A neural emulator network to represent the minimized cumulative structural responses under

[1]Assoc. Prof., Dept. of Civ. Engrg., Nat. Chiao Tung Univ., 1001 Ta Hsueh Rd., Hsinchu Taiwan 300, Republic of China. E-mail: slhung@cc.nctu.edu.tw

[2]PhD Candidate, Dept. of Civ. Engrg., Nat. Chiao Tung Univ., 1001 Ta Hsueh Rd., Hsinchu Taiwan 300, Republic of China.

[3]Grad. Student, Dept. of Civ. Engrg., Nat. Chiao Tung Univ., 1001 Ta Hsueh Rd., Hsinchu Taiwan 300, Republic of China.

Note. Associate Editor: Dimitrios Karamanlidis. Discussion open until January 1, 2001. To extend the closing date one month, a written request must be filled with the ASCE Manager of Journals. The manuscript for this paper was submitted for review and possible publication on June 8, 1998. This paper is part of the ***Journal of Engineering Mechanics***, Vol. 126, No. 8, August, 2000. ©ASCE, ISSN 0733-9399/00/0008-0839–0849/$8.00 + $.50 per page. Paper No. 18512.

both the seismic loading and the pulse control force; and (2) a neural control network to determine the pulse control force on the structure. The control effectiveness of the ANSAP controller using the L-BFGS and a modified BP algorithm in neural emulator network and the instantaneous optimal control algorithm is first investigated for a single-degree-of-freedom (SDOF) structure subjected to the El Centro earthquake. Furthermore, the feasibility of the ANSAP controller is evaluated by a sample three-story structure subjected to the El Centro and the Pacoima earthquakes.

ARTIFICIAL NEURAL NETWORKS

Artificial neural networks (ANNs) form a class of systems that are inspired by biological neural networks. The topology of an ANN model consists of a number of simple processing elements, called nodes, that are interconnected to each other. Interconnection weights that represent the information stored in the system are used to quantify the strength of the interconnections; these weights hold the key to the functioning of an ANN. Among the many different types of ANN, the feedforward, multilayered, supervised neural network with the error back-propagation algorithm, the so-called back-propagation (BP) network (Rumelhart et al. 1986), is by far the most commonly applied neural network learning model, due to its simplicity. Before an ANN can be used in the application, it needs to learn or be trained from an existing database consisting of pairs of input-output patterns. The topology of BP networks consists of an input layer, one or more hidden layers, and an output layer. The training of a supervised neural network usually involves three stages. The first stage is the data feedforward. The output of each node is defined as follows:

$$\text{net}_j = \sum_{i=1}^{n} W_{ij} X_i + \theta_j \tag{1}$$

$$o_j = f(\text{net}_j) \tag{2}$$

where W_{ij} is the weight associated with the ith node in the preceding layer to the jth node in the current layer; X_i is the output of the ith node in the preceding layer; θ_j is the threshold value of node j in the current layer; o_j is the output of node j in the current layer; and function f is the activation function, which has to be differentiable. Herein, the hyperbolic tangent function is used as the activation function and is defined as follows:

$$f(x) = \frac{e^x - e^{-x}}{e^x + e^{-x}} \tag{3}$$

The second stage is error back-propagation through the network. In the training process, system error function is used to monitor the learning performance of the network. This system error function is defined as follows:

$$E = \frac{1}{2P} \sum_{p=1}^{P} \sum_{k=1}^{K} (d_{pk} - o_{pk})^2 \tag{4}$$

where P is the number of instances in the training set and d_{pk} as well as o_{pk} are the desired and calculated output of the kth output node for the pth instance, respectively. The final stage is the adjustment of the weights. The standard BP algorithm uses a gradient descent approach with a constant step length (learning ratio) to train the network.

$$W_{ij}^{(k+1)} = W_{ij}^{(k)} + \Delta W_{ij} \tag{5}$$

$$\Delta W_{ij} = -\eta \frac{\partial E}{\partial W_{ij}} \tag{6}$$

where η is the learning ratio, a constant in the range of [0, 1]. The superscript index (k) denotes the kth learning iteration. BP supervised neural network learning models, however, always take a long time to learn (Adeli and Hung 1995). Moreover, the convergence of a BP neural network is highly dependent upon the use of a learning rate (η). Thus, several different approaches developed to enhance the learning performance of the BP learning algorithm have been applied (Adeli and Hung 1995).

Hung and Lin (1994) developed a more effective adaptive L-BFGS learning algorithm based on the approach of an L-BFGS quasi-Newton second-order method (Nocedal 1980) with an inexact line search algorithm. In the conventional BFGS method, the approximation $\mathbf{H}_{k+1}$ to the inverse Hessian matrix of function $E(\mathbf{W})$ is updated by

$$\mathbf{H}_{k+1} = (\mathbf{I} - \rho_k \mathbf{s}_k \mathbf{y}_k^T)\mathbf{H}_k(\mathbf{I} - \rho_k \mathbf{y}_k \mathbf{s}_k^T) + \rho_k \mathbf{s}_k \mathbf{s}_k^T \tag{7a}$$

$$\mathbf{H}_{k+1} \equiv \mathbf{V}_k^T \mathbf{H}_k \mathbf{V}_k + \rho_k \mathbf{s}_k \mathbf{s}_k^T \tag{7b}$$

where

$$\rho_k = 1/\mathbf{y}_k^T \mathbf{s}_k \tag{8}$$

$$\mathbf{V}_k = \mathbf{I} - \rho_k \mathbf{y}_k \mathbf{s}_k^T \tag{9}$$

$$\mathbf{s}_k = \mathbf{W}_{k+1} - \mathbf{W}_k \tag{10}$$

$$\mathbf{y}_k = \mathbf{g}_{k+1} - \mathbf{g}_k \tag{11}$$

$$\mathbf{g}_k = \frac{\partial E}{\partial \mathbf{W}} \tag{12}$$

Instead of forming the matrix $\mathbf{H}_k$ in the BFGS method, we save the vectors $\mathbf{s}_k$ and $\mathbf{y}_k$. These vectors first define and then implicitly and dynamically update the Hessian approximation using information from the last few iterations, say, m in the work. Therefore, the final stage of the adjustment of the weights is modified as follows:

$$\mathbf{W}^{(k+1)} = \mathbf{W}^{(k)} + \alpha_k \mathbf{d}_k \tag{13}$$

The search direction is given by

$$\mathbf{d}_k = -\mathbf{H}_k \mathbf{g}_k + \beta_k \mathbf{d}_{k-1} \tag{14}$$

where

$$\beta_k = \frac{\mathbf{y}_{(k-1)}^T \mathbf{H}_{(k-1)} \mathbf{g}_{(k-1)}}{\mathbf{y}_{(k-1)}^T \mathbf{d}_{(k-1)}} \tag{15}$$

The step length, α_k, is adapted during the learning process through a mathematical approach: the inexact line search algorithm. This is used in the L-BFGS learning algorithm instead of a constant learning ratio (Hung and Lin 1994; Adeli and Hung 1995). The inexact line search algorithm is based on three sequential approaches: bracketing, sectioning, and interpolation. Consequently, the step length α_k is required to satisfy the following conditions in each iteration (Hung and Lin 1994):

$$E(\mathbf{W}_k + \alpha_k \mathbf{d}_k) \le E(\mathbf{W}_k) + \beta \alpha_k (\nabla E(\mathbf{W}_k)^T \mathbf{d}_k) \quad \beta \in (0, 1) \text{ and } \alpha_k > 0 \tag{16}$$

$$\nabla E(\mathbf{W}_k + \alpha_k \mathbf{d}_k)^T \mathbf{d}_k \ge \theta (\nabla E(\mathbf{W}_k)^T \mathbf{d}_k) \quad \theta \in (\beta, 1) \text{ and } \alpha_k > 0 \tag{17}$$

$$\nabla E(\mathbf{W}_k + \alpha_k \mathbf{d}_k)^T \mathbf{d}_{(k+1)} < 0 \tag{18}$$

Hence, the problem of trial-and-error selection of a learning ratio in the standard BP algorithm is circumvented in the adaptive L-BFGS learning algorithm.

CLASSICAL CLOSED-LOOP OPTIMAL CONTROL ALGORITHM

Active control in civil engineering structures is based on closed-loop control, implying that the structural response is

J. Eng. Mech. 2000.126:839-849.

continually monitored and this information is used to continuously modify the applied control forces. The responses of a system with a linear n-degree-of-freedom structure, when the system is subjected in an external excitation in configuration space, can be described by the following equation:

$$\mathbf{M}\ddot{\underline{\mathbf{x}}}(t) + \mathbf{C}\dot{\underline{\mathbf{x}}}(t) + \mathbf{K}\underline{\mathbf{x}}(t) = \mathbf{B}_1\underline{\mathbf{u}}(t) + \mathbf{E}_1\underline{\mathbf{w}}(t) \tag{19}$$

where constant matrices $\mathbf{M}$, $\mathbf{C}$, and $\mathbf{K}$ are, respectively, the mass, damping, and stiffness matrices with $n \times n$ entities; $\underline{\mathbf{x}}(t)$ is the n-dimensional displacement vector with respect to the ground; $\underline{\mathbf{u}}(t)$ is the p-dimensional control force vector; $\underline{\mathbf{w}}(t)$ is the q-dimensional external excitation vector; and the $n \times p$ matrix $\mathbf{B}_1$ and $n \times q$ matrix $\mathbf{E}_1$ are location matrices that define the locations of the control force and the excitation, respectively. While assuming that the control force and external excitation are constants in any sampling period Δt, (19) can be written in a discrete state equation as follows:

$$\underline{\mathbf{z}}[k+1] = \mathbf{A}_d\underline{\mathbf{z}}[k] + \mathbf{B}_d\underline{\mathbf{u}}[k] + \mathbf{E}_d\underline{\mathbf{w}}[k] \tag{20}$$

where $\mathbf{A}_d = e^{\mathbf{A}\Delta t}$; $\mathbf{B}_d = \mathbf{A}^{-1}(\mathbf{A}_d - \mathbf{I})\mathbf{B}$; and $\mathbf{E}_d = \mathbf{A}^{-1}(\mathbf{A}_d - \mathbf{I})\mathbf{E}$. Index k is an integer number; $k = 0, 1, 2, \ldots, N$;

$$\underline{\mathbf{z}}[k+1] = \begin{bmatrix} \underline{\mathbf{x}}[k+1] \\ \dot{\underline{\mathbf{x}}}[k+1] \end{bmatrix}_{2n\times 1}$$

is a $2n$-dimensional state vector of the structure response at time $t = (k+1)\Delta t$, and Δt is the time length of the sampling period. The matrices $\mathbf{A}$, $\mathbf{B}$, and $\mathbf{E}$ can be determined by the following:

$$\mathbf{A} = \begin{bmatrix} 0 & \mathbf{I} \\ -\mathbf{M}^{-1}\mathbf{K} & -\mathbf{M}^{-1}\mathbf{C} \end{bmatrix}_{2n\times 2n} \tag{21}$$

$$\mathbf{B} = \begin{bmatrix} 0 \\ \mathbf{M}^{-1}\mathbf{B}_1 \end{bmatrix}_{2n\times p} \tag{22}$$

$$\mathbf{E} = \begin{bmatrix} 0 \\ \mathbf{M}^{-1}\mathbf{E}_1 \end{bmatrix}_{2n\times q} \tag{23}$$

The control force, in general, is designed to be a function of the measured displacement and velocity vectors and can be expressed as a linear combination of measured structure response in a discrete state equation as follows:

$$\underline{\mathbf{u}}[k] = \mathbf{G}_1\underline{\mathbf{x}}[k] + \mathbf{G}_2\dot{\underline{\mathbf{x}}}[k] = \mathbf{G}\underline{\mathbf{z}}[k] \tag{24}$$

where $\mathbf{G}_1$ and $\mathbf{G}_2$ are the feedback gain matrices of displacement and velocity, respectively, and $\mathbf{G}$ is a constant gain matrix.

ACTIVE PULSE CONTROL ALGORITHM

In the active pulse control algorithm, the pulse control force applied to the structure is reduced in a $\Delta t_u (\Delta t_u < \Delta t)$ period, as displayed in Fig. 1. Furthermore, the effect of pulses is assumed to be postponed to just before the next sampling time. Consequently, there is time to calculate the control force during the former $\Delta t - \Delta t_u$ period and to apply it to the structure during the later Δt_u period of each time step Δt. Thus, the problem of time delay effect due to the computation time was circumvented in the proposed control strategy. According to Fig. 1, assuming that the external seismic force and the control force are piecewise-linear and piecewise-constant interpolation functions, respectively, they can be expressed in the following forms:

$$\underline{\mathbf{u}}(\tau) = 0, \quad k\Delta t \le \tau < [(k+1)\Delta t - \Delta t_u] \tag{25}$$

$$\underline{\mathbf{u}}(\tau) = \underline{\mathbf{u}}[k\Delta t], \quad [(k+1)\Delta t - \Delta t_u] \le \tau < (k+1)\Delta t \tag{26}$$

$$\underline{\mathbf{w}}(\tau) = \frac{\tau - k\Delta t}{\Delta t}\{\underline{\mathbf{w}}[(k+1)\Delta t] - \underline{\mathbf{w}}[k\Delta t]\} + \underline{\mathbf{w}}[k\Delta t], \quad k\Delta t \le \tau < (k+1)\Delta t \tag{27}$$

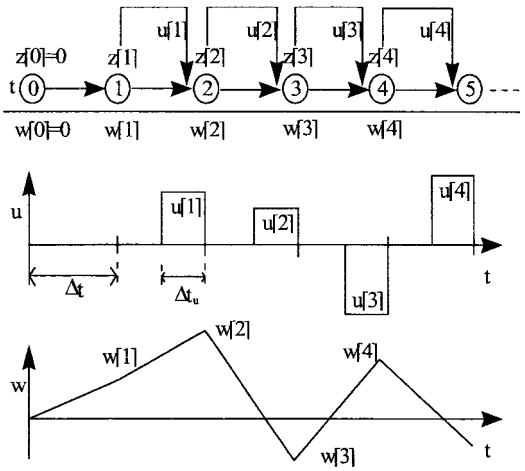

FIG. 1. Basic Assumptions of Applying Pulse Control Force

Therefore, (20) can be rewritten as follows:

$$\underline{\mathbf{z}}[k+1] = \mathbf{A}_p\underline{\mathbf{z}}[k] + \mathbf{B}_p\mathbf{B}\underline{\mathbf{u}}[k] + \mathbf{E}_{p1}\mathbf{E}\underline{\mathbf{w}}[k+1] + \mathbf{E}_{p2}\mathbf{E}(\mathbf{w}[k+1] - \underline{\mathbf{w}}[k]) \tag{28}$$

where $\mathbf{A}_p = e^{\mathbf{A}\Delta t_u}$, $\mathbf{B}_p = \mathbf{A}^{-1}(e^{\mathbf{A}\Delta t_u} - \mathbf{I})$, $\mathbf{E}_{p1} = \mathbf{A}^{-1}(\mathbf{A}_p - \mathbf{I})$, and $\mathbf{E}_{p2} = \mathbf{A}^{-1}[(\mathbf{E}_{p1}/\Delta t) - \mathbf{A}_p]$.

The main notion of an active pulse control system is to destroy the gradual rhythmic buildup of the structural response by applying pulses of suitable magnitude and proper direction. Thus, the proposed control strategy is to apply the control force to minimize the system response that carries over from the current time step to the next time step. The first two terms in the right-hand side of (28) represent the structural response at time $k(\Delta t)$ after the active pulse force $\underline{\mathbf{u}}[k]$ has been applied. That is, the structural response $\underline{\mathbf{z}}[k]$ at any time $k(\Delta t)$ should be eliminated by applying a pulse control force $\underline{\mathbf{u}}[k]$.

$$\underline{\mathbf{z}}^*[k] = \mathbf{A}_p\underline{\mathbf{z}}[k] + \mathbf{B}_p\mathbf{B}\underline{\mathbf{u}}[k] = 0 \tag{29}$$

The control force can be obtained as

$$\underline{\mathbf{u}}[k] = -(\mathbf{B}^T\mathbf{B})^{-1}\mathbf{B}^T\mathbf{B}_p^{-1}\mathbf{A}_p\underline{\mathbf{z}}[k] = \mathbf{G}\underline{\mathbf{z}}[k] \tag{30}$$

The matrix $\mathbf{G}$ is called a state feedback gain matrix and equates to

$$\mathbf{G} = -(\mathbf{B}^T\mathbf{B})^{-1}\mathbf{B}^T\mathbf{B}_p^{-1}\mathbf{A}_p \tag{31}$$

ADAPTIVE NEURAL STRUCTURAL ACTIVE PULSE (ANSAP) CONTROLLER

For simplicity, assume that only one active tendon controller is used and that it can be used on any floor. After controlling each degree of freedom, all the relative displacements and relative velocities of the structure cannot be kept at zero by a single pulse control force, but minimizing the cumulative structural responses allows us to apply the single pulse control force. Hence, modifying the control strategy is an attempt to minimize the cumulative structural responses, $\underline{\mathbf{z}}^*[k]$ in (29), by applying the pulse control force. The simplest way to achieve this aim is to minimize the sum of the square of the cumulative structural responses, which happens to be an unconstrained optimization problem, solved most effectively using supervised ANN models.

The ANSAP controller, schematically presented in Fig. 2, consists of two components: (1) A neural emulator network to represent the minimized cumulative structural responses under both the seismic loading and the pulse control force; and (2) a neural control network to determine the pulse control force on the structure. The details of these two components of the ANSAP controller are presented in the following.

J. Eng. Mech. 2000.126:839-849.

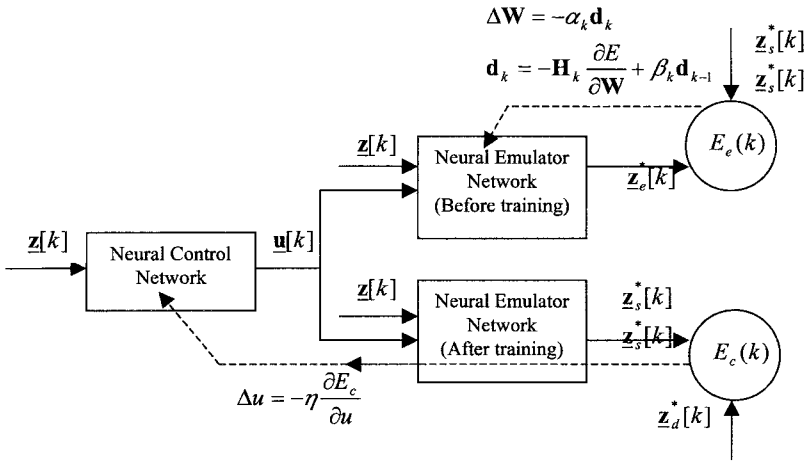

FIG. 2. Structure and Training of ANSAP Controller

Neural Emulator Network

This network is modeled by an adaptive L-BFGS neural network model, which models the dynamic behavior of the structure described by (29). To minimize the sum of the square of the cumulative structural responses, vectors $\underline{\mathbf{u}}[k]$ and $\underline{\mathbf{z}}[k]$ are the inputs, and vector $\underline{\mathbf{z}}^*[k]$ is the corresponding output of the neural emulator network. The input data of the training instances are generated randomly and are substituted into (29) to generate the desired outputs of the training instances. The computed outputs are then generated by feeding the inputs forward through the network. The difference between the desired and computed outputs, $\underline{\mathbf{z}}_e^*[k]$ and $\underline{\mathbf{z}}_s^*[k]$, of the neural emulator network is then measured. Finally, the weights of the network are adjusted based on the error function $E_e(k)$. After the system error converges to a desired value, the neural emulator network can model the dynamic behavior of the real structure.

Neural Control Network

The neural control network searches for a proper state feedback gain matrix $\mathbf{G}$ to get a suitable pulse control force to minimize the cumulative structural responses $\underline{\mathbf{z}}_e^*[k]$. Eq. (30) indicates that the pulse control force is proportional to the state feedback gain matrix $\mathbf{G}$ and the state of structure $\underline{\mathbf{z}}[k]$; thus the input and the corresponding output to the neural control network are vectors $\underline{\mathbf{z}}[k]$ and $\underline{\mathbf{u}}[k]$, respectively. In this study, a modified BP (a conventional BP with an inexact line search algorithm) neural network is adopted as the neural control network for computational and memory storage efficiency.

Before the neural control network can be trained, the neural emulator network has to be trained to represent the performance of a real structure. The training process of the neural control network is also demonstrated in Fig. 2. First, the input vector $\underline{\mathbf{z}}[k]$ is presented to the neutral control network to compute the pulse control force $\underline{\mathbf{u}}[k]$, which is then applied to the pretrained neural emulator network to obtain the minimized cumulative response $\underline{\mathbf{z}}_s^*[k]$. The error function $E_c(k)$ can be formulated as follows:

$$E_c(k) = \frac{1}{2P} \sum_{p=1}^{P} \sum_{0} [\underline{\mathbf{z}}_{pd}^{*o}[k] - \underline{\mathbf{z}}_{ps}^{*o}[k]]^2 \tag{32}$$

where P is the number of instances in the training set; and $\underline{\mathbf{z}}_{pd}^{*[k]}$ is the desired minimized cumulative responses of the structure to be controlled, chosen to be zero in this work. The superscript o represents the oth element of the output vectors. Second, the weights W_{ij}^C in the neural control network are then updated as follows:

$$\Delta W_{ij}^C = -\eta \frac{\partial E_c}{\partial W_{ij}^C} \tag{33}$$

$$\Delta W_{ij}^C = -\eta \sum_k \left(\frac{\partial E_c}{\partial u_k}\right)\left(\frac{\partial u_k}{\partial W_{ij}^C}\right) \tag{34}$$

Herein, the learning ratio η is dynamically determined via the inexact line search algorithm. Term u_k is the kth component of the pulse control force, $\underline{\mathbf{u}}$. Eq. (34) indicates that the adjustment of the weight W_{ij}^C during the training process is split into two steps: First back-propagating the system error function E_c through the pretrained neural emulator network without any changes in the weights W_{ij}^E to calculate the corresponding error Δu of the pulse control force $\underline{\mathbf{u}}$; then back-propagating the error Δu through the neural control network to adjust the weights W_{ij}^C. The training process is terminated as the minimized cumulative structural responses converge to the desired responses within the predetermined tolerance.

NUMERICAL EXAMPLES

Example 1

Herein, an SDOF system was chosen as the structure to be controlled in order to compare the control effectiveness of the following four cases:

- Case 1: ANSAP controller using modified BP learning algorithm in both the neural control network and neural emulator network.
- Case 2: ANSAP controller with neural control network using modified BP learning algorithm and neural emulator network using L-BGFS learning algorithm.
- Case 3: The neurocontroller proposed by Tang (1995).
- Case 4: Instantaneous optimal closed-loop control algorithm (Soong 1990).

This structure is an approximately 1:4 scale model of a 1:2 scale model of the prototype structure. The properties of the SDOF system are given in Table 1. Response spectra for the

TABLE 1. System Parameter Values for SDOF Example

Parameter (1)	Quantity (2)
Mass (m)	2,923.38 kg
Structure stiffness (k)	1,391.06 kN/m
Natural frequency (f_0)	3.47 Hz
Damping factor (ζ)	5%
Damping coefficient (c)	6,373.74 N·s/m

J. Eng. Mech. 2000.126:839-849.

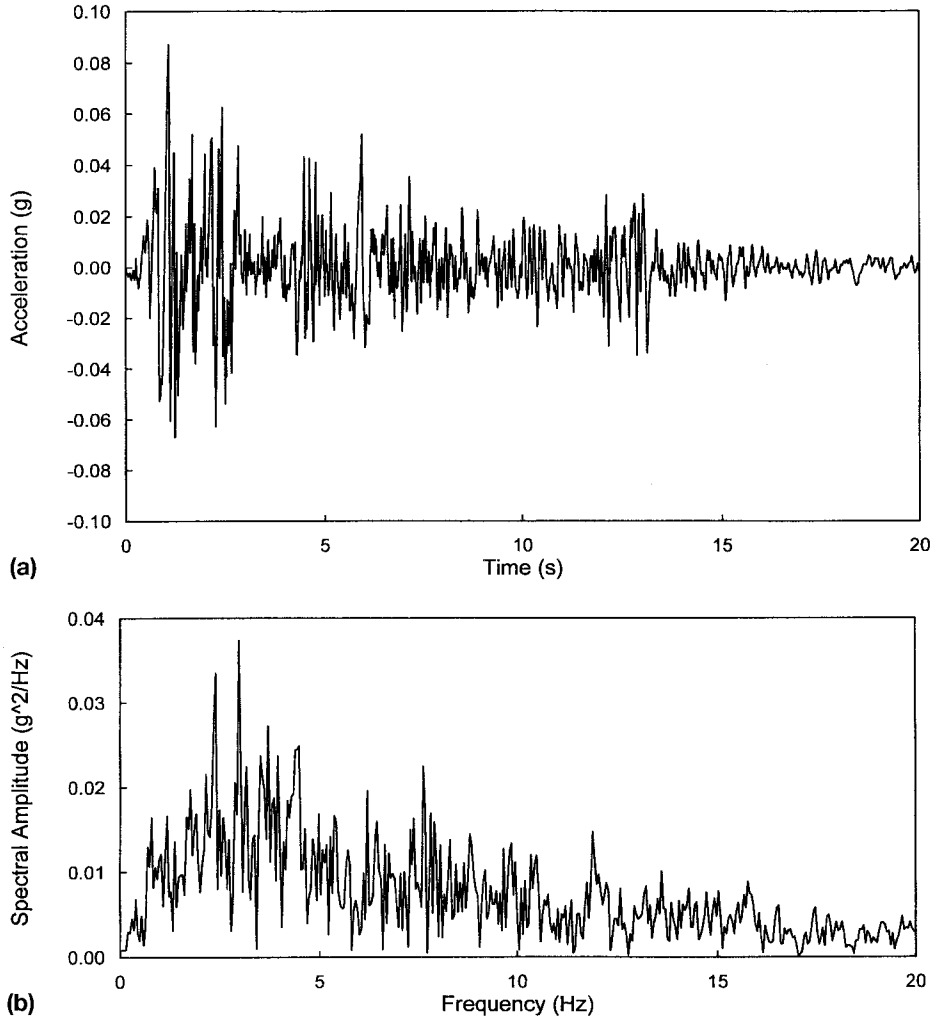

FIG. 3. (a) Time History; (b) Acceleration Spectrum of Base Motion One

1940 El Centro earthquake record, referred to as base motion one, were used as the external excitation, but scaled to 25% of the intensity of the original earthquake. The sampling period Δt is 0.01 s. Fig. 3 displays the time history and the corresponding acceleration spectra of base motion one.

First, case 1 is compared with case 2. The pulse duration Δt_u is assumed to be half of Δt. The training data set of both the neural emulator and the control networks is the first 1,000 records of base motion one for the two cases. Fig. 4 displays the flow chart of the processes of training and analyzing the ANSAP controller. The neural emulator network trained consists of three, seven, and two nodes in the input layer, hidden layer, and output layer, respectively, and denoted as NEN_BP(3-7-2) for case 1 and NEN_L-BFGS(3-7-2) for case 2. The three input data are the structural relative displacement $\underline{x}[k]$, relative velocity $\underline{\dot{x}}[k]$, and one control force $\underline{\mathbf{u}}[k]$. The two outputs are the cumulative structural relative displacement $\underline{x}^*[k]$ and relative velocity $\underline{\dot{x}}^*[k]$. The complete off-line training process takes approximate 400 cycles, and the system error converges to 0.000354 for case 1, compared with 30 cycles and system error converging to 0.000042 for case 2. Results show that L-BFGS is considerably faster than modified BP.

After the neural emulator network is obtained, the neural control network is then trained. The neural control network in this example is constructed with two, two, and one nodes in the input, hidden, and output layers, respectively, and denoted as NCN_BP(2-2-1) for both cases. The two input data of the network are designated to be the structural relative displacement $\underline{x}[k]$ and relative velocity $\underline{\dot{x}}[k]$. The only output of the neural control network is the control force $\underline{\mathbf{u}}[k]$. The entire off-line training process takes about 500 cycles, and the system error converges to 0.000268 for both cases.

After the ANSAP controller is trained, it is then tested. The testing data set is the 2,000 records of base motion one. Fig. 5 presents the relative displacements of controlled and uncontrolled excitation under base motion one. It reveals that both cases destroy the gradual rhythmic buildup of the structural response, and case 2 is slightly more efficient than case 1.

Second, the last two cases are compared with the first two cases. Case 3 is the neurocontroller proposed by Tang. The neurocontroller is a simple heuristic-based control strategy capable of applying the control force to cancel the system velocity at the preceding time step for a single-degree-of-freedom system. Case 4 is the instantaneous optimal closed-loop control algorithm (Soong 1990) in which the structure responses and active control force depend on the weighting matrices **Q** and **R**. Table 2 lists the controlled relative displacements of all the four cases at the peak of uncontrolled displacements. In this example, the maximum uncontrolled relative displacement is 0.46 cm (at 1.11 s). After control, the displacement is reduced to 0.064, 0.055, 0.058, 0.053, and 0.075 cm for cases 1, 2, 3, 4-1, and 4-2, respectively. These data indicate that all four cases can significantly reduce the structural responses at the peak of the displacements (PD). The control effectiveness of case 3 is almost as effective as that of the first two cases, while whether that of case 4 may be better or worse than the first two cases depends on the choice of the

J. Eng. Mech. 2000.126:839-849.

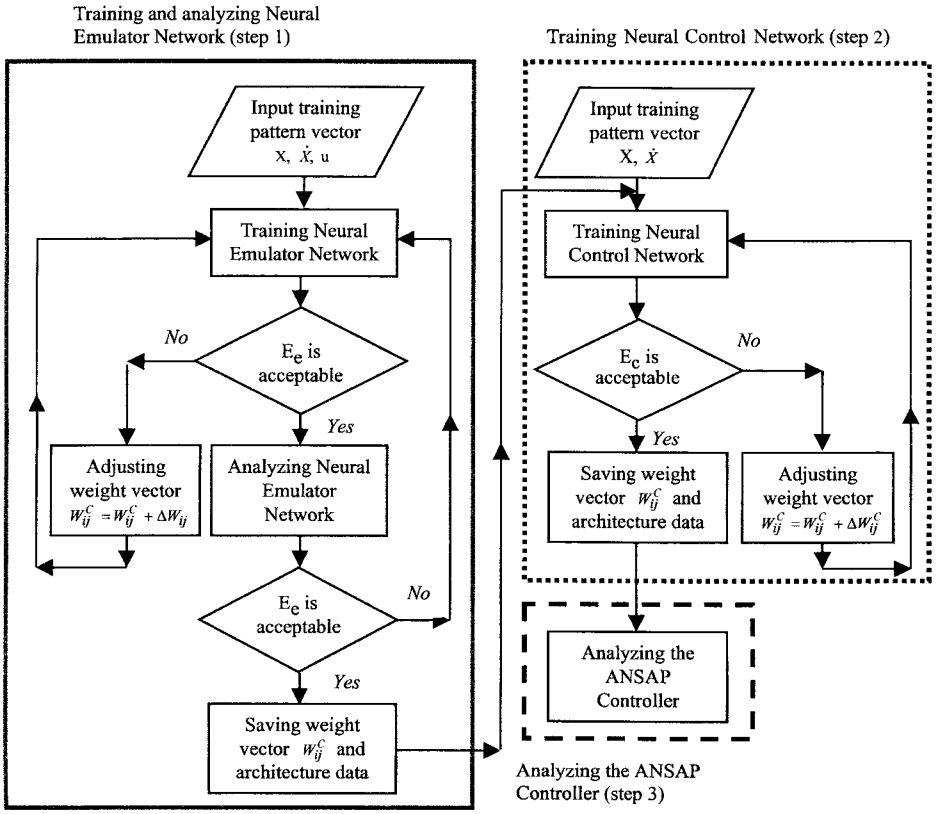

FIG. 4. Flow Chart for Control Strategy of ANSAP Controller

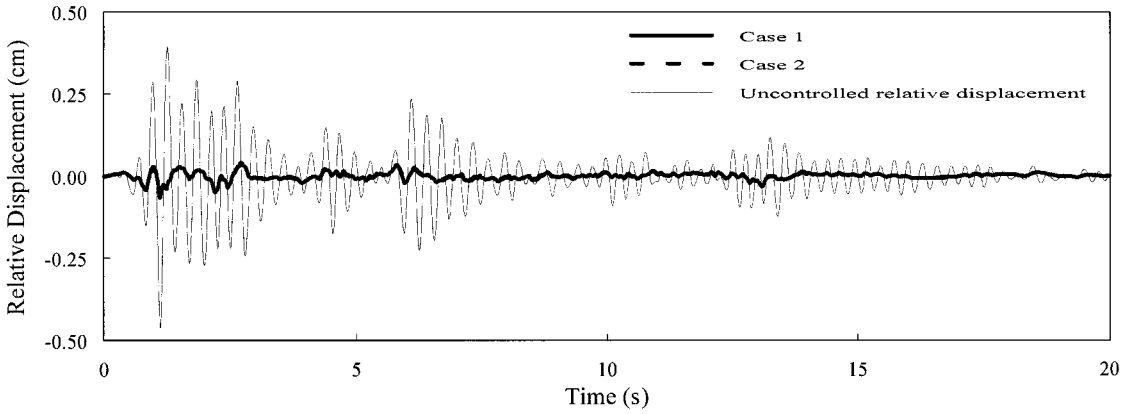

FIG. 5. Comparison of Uncontrolled and Controlled Relative Displacements of Case 1 and Case 2 (Input: Base Motion One)

TABLE 2. Controlled Relative Displacements of All Four Cases at Peak of Uncontrolled Displacements

Cases (1)	Parameter *R* (2)	Parameter *Q* (3)	Controlled relative displacement at PD (cm) (4)
Case 1	—	—	0.064
Case 2	—	—	0.055
Case 3	—	—	0.058
Case 4			
Case 4-1	1	$\begin{bmatrix} 0 & 0 \\ 120{,}000 & 120{,}000 \end{bmatrix}$	0.053
Case 4-2	1	$\begin{bmatrix} 0 & 0 \\ 80{,}000 & 80{,}000 \end{bmatrix}$	0.075

weighting matrices **Q** and **R**. Notably, the first three cases consider time delay effect, but the last one doesn't.

Example 2

ANSAP Controller Training

In this example, a three-degree-of-freedom linear structure system is chosen to explore the control effectiveness of the proposed control strategy and the feasibility of the active structural control using the ANSAP controller in MDOF structure systems. Fig. 6 depicts the three-story structure, with an active tendon controller installed on the first floor. The structural properties are listed in Table 3. The responses of the structure are the displacements and velocities with respect to the ground of each floor. The base motion one is used for training both

J. Eng. Mech. 2000.126:839-849.

the neural emulator and control networks. The pulse duration Δt_u is also half of sampling period Δt; that is, $\Delta t_u = 0.005$ s.

The training data set of both the neural emulator and the control networks is the 2,000 records of base motion one. The topology of the neural emulator network trained in this example is seven, seven, and six nodes in the input, hidden, and output layers, respectively, and denoted as NEN_L-BFGS(7-7-6). The seven input data are the relative displacements and relative velocities of each floor $x_1[k]$, $x_2[k]$, $x_3[k]$, $\dot{x}_1[k]$, $\dot{x}_2[k]$, and $\dot{x}_3[k]$ and one control force $\underline{\mathbf{u}}[k]$. The six outputs are the cumulative relative displacements and relative velocities of each floor $x_1^*[k]$, $x_2^*[k]$, $x_3^*[k]$, $\dot{x}_1^*[k]$, $\dot{x}_2^*[k]$, and $\dot{x}_3^*[k]$. The complete off-line training process takes approximate 300 cycles, and the system error converges to 0.00027.

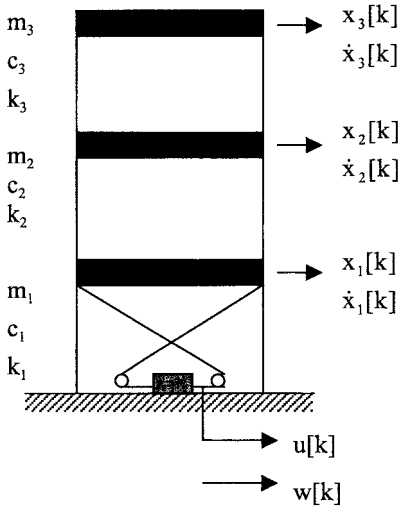

FIG. 6. Three-Story Structure System

TABLE 3. System Parameter Values for MDOF Example

Parameter (1)	Quantity (2)
Mass matrix (**M**)	$\begin{bmatrix} 2{,}923.38 & 0 & 0 \\ 0 & 2{,}923.38 & 0 \\ 0 & 0 & 2{,}923.38 \end{bmatrix}$ kg
Structure stiffness matrix (**K**)	$\begin{bmatrix} 2{,}782.12 & -1{,}391.06 & 0 \\ -1{,}391.06 & 2{,}782.12 & -1{,}391.06 \\ 0 & -1{,}391.06 & 1{,}391.06 \end{bmatrix}$ kN/m
Damping matrix (**C**)	$\begin{bmatrix} 12{,}747.48 & -6{,}373.74 & 0 \\ -6{,}373.74 & 12{,}747.48 & -6{,}373.74 \\ 0 & -6{,}373.74 & 6{,}373.74 \end{bmatrix}$ N·s/m

After the neural emulator network is obtained, the neural control network is then trained. The neural control network in this example is constructed with six, three, and one nodes in the input, hidden, and output layers, respectively, and denoted as NCN_BP(6-3-1). The six input data are the relative displacements and relative velocities of each floor $x_1[k]$, $x_2[k]$, $x_3[k]$, $\dot{x}_1[k]$, $\dot{x}_2[k]$, and $\dot{x}_3[k]$. The output of the neural control network is the control force $\underline{\mathbf{u}}[k]$. The entire off-line training process takes about 1,000 cycles, and the system error converges to 0.0496. Figs. 7–9 display the relative displacements, with controlled and uncontrolled excitation, for each floor of the three-story structure. The maximum uncontrolled relative displacements of the first, second, and third floors of the three-story structure are 0.385 cm (at 3.08 s), 0.685 cm (at 3.07 s), and 0.880 cm (at 3.05 s), respectively. After control, these relative displacements are reduced to 0.0275, 0.244, and 0.439 cm, respectively. The example results indicate that the structural responses are significantly reduced at the peak of the relative displacements. Fig. 10 illustrates the time history of the external applied pulse control force.

ANSAP Controller Testing

After the ANSAP controller is trained using the El Centro earthquake, another earthquake motion, the Pacoima earthquake, is used to verify the control ability of the ANSAP controller in handling the uncertainty about the time history of the excitation. For the sake of factorization, the Pacoima earthquake, referred to as base motion two, is also scaled to 25% of the intensity of the El Centro earthquake. Fig. 11 displays the time history and the corresponding response spectra of base motion two. The testing data set of the control network is the 1990 records of base motion two. Figs. 12–14 present the relative displacements of controlled and uncontrolled excitation for each floor of the three-story structure under base motion two. In this case, the maximum uncontrolled displacements of the first, second, and third floors of the three-story structure are 0.435 cm (at 2.50 s), 0.773 cm (at 2.50 s), and 0.977 cm (at 2.16 s), respectively. After control, these relative displacements are reduced to 0.0127, 0.144, and 0.108 cm, respectively. These data also indicate that the structural responses are significantly reduced at the peak of the relative displacements, even though the ANSAP controller is trained on base motion one. Fig. 15 illustrates the time history of the computed pulse control force. The acceleration response spectra of the El Centro earthquake and the Pacoima earthquake, displayed in Figs. 3 and 11, respectively, are entirely different. Remarkably, the performance of the ANSAP controller trained using the recorded data of the El Centro earthquake is also practical for addressing the Pacoima earthquake, although

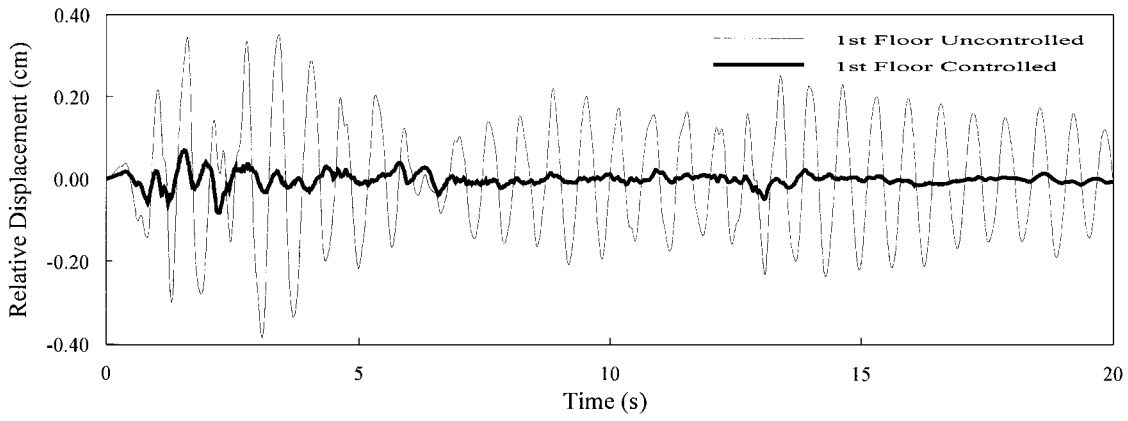

FIG. 7. Controlled and Uncontrolled Relative Displacements of First Floor of Three-Story Structure Subjected to Base Motion One

J. Eng. Mech. 2000.126:839-849.

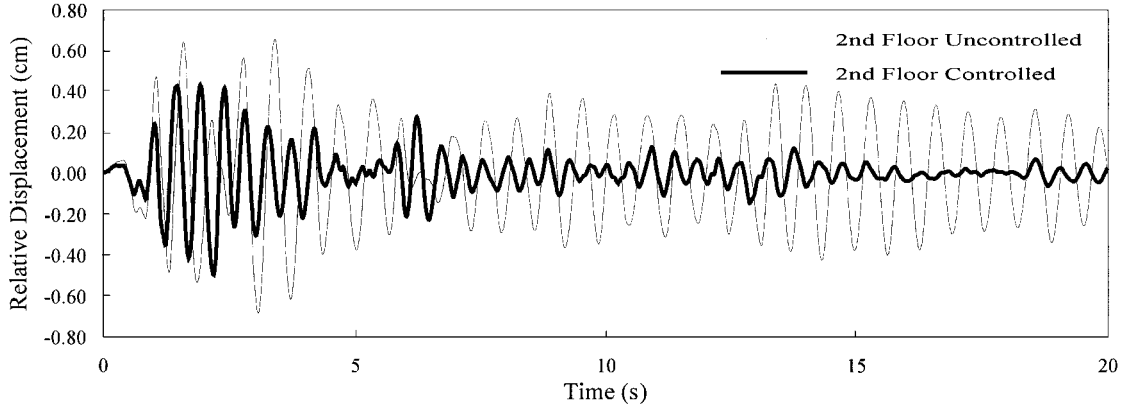

FIG. 8. Controlled and Uncontrolled Relative Displacements of Second Floor of Three-Story Structure Subjected to Base Motion One

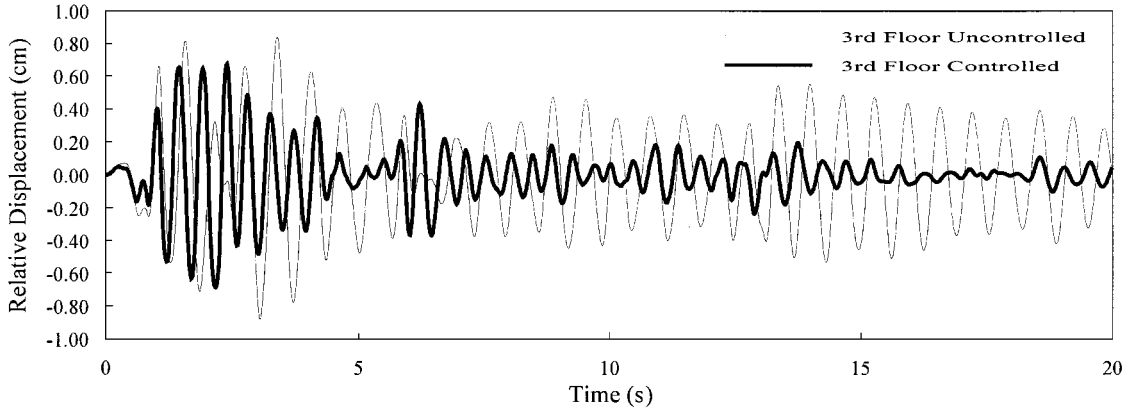

FIG. 9. Controlled and Uncontrolled Relative Displacements of Third Floor of Three-Story Structure Subjected to Base Motion One

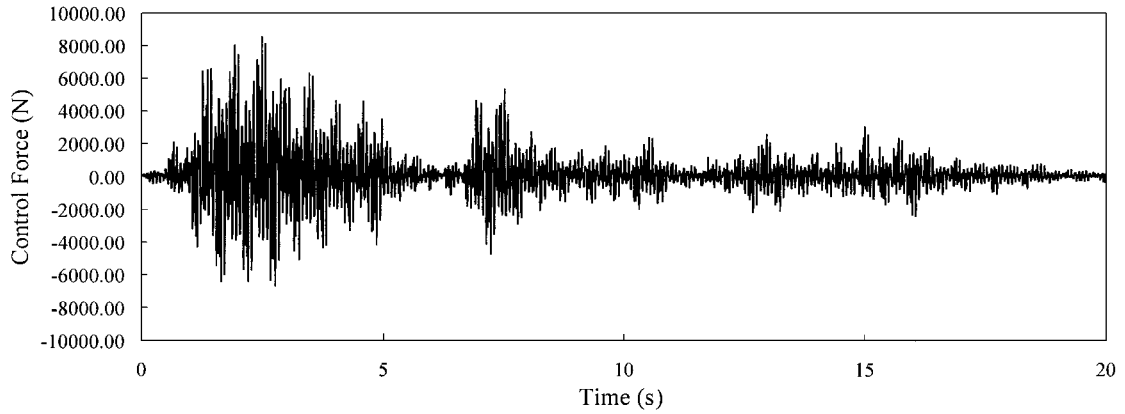

FIG. 10. Time History of Pulse Control Force for Three-Story Structure Subjected to Base Motion One

there are many differences in the peak, shape, and amplitude of the spectra of the two earthquakes.

Control Effectiveness of ANSAP Controller

To evaluate the control effectiveness of the ANSAP controller, the term control index is defined as

$$I_c = 1 - \frac{\sum_{k=1}^{N} (\underline{x}_c[k])^2}{\sum_{K=1}^{N} (\underline{x}_u[k])^2} \tag{35}$$

where $\underline{x}_c[k]$ = controlled relative displacements of the structure; and $\underline{x}_u[k]$ = uncontrolled relative displacements of the structure.

For $\underline{x}_c \leq \underline{x}_u$, the range of values of I_c may vary from a minimum of 0 for no control to a maximum of 1 for the optimum control condition ($\underline{x}_c = 0$ during the entire time history). If $\underline{x}_c$ is half of $\underline{x}_u$ during the entire time history, the control index I_c equals 0.75. A larger I_c implies a better control effectiveness.

In the numerical examples, the control indices I_c equal 0.987, 0.805, and 0.692 for the first, second, and third floors of the structure, respectively, subjected to base motion one.

J. Eng. Mech. 2000.126:839-849.

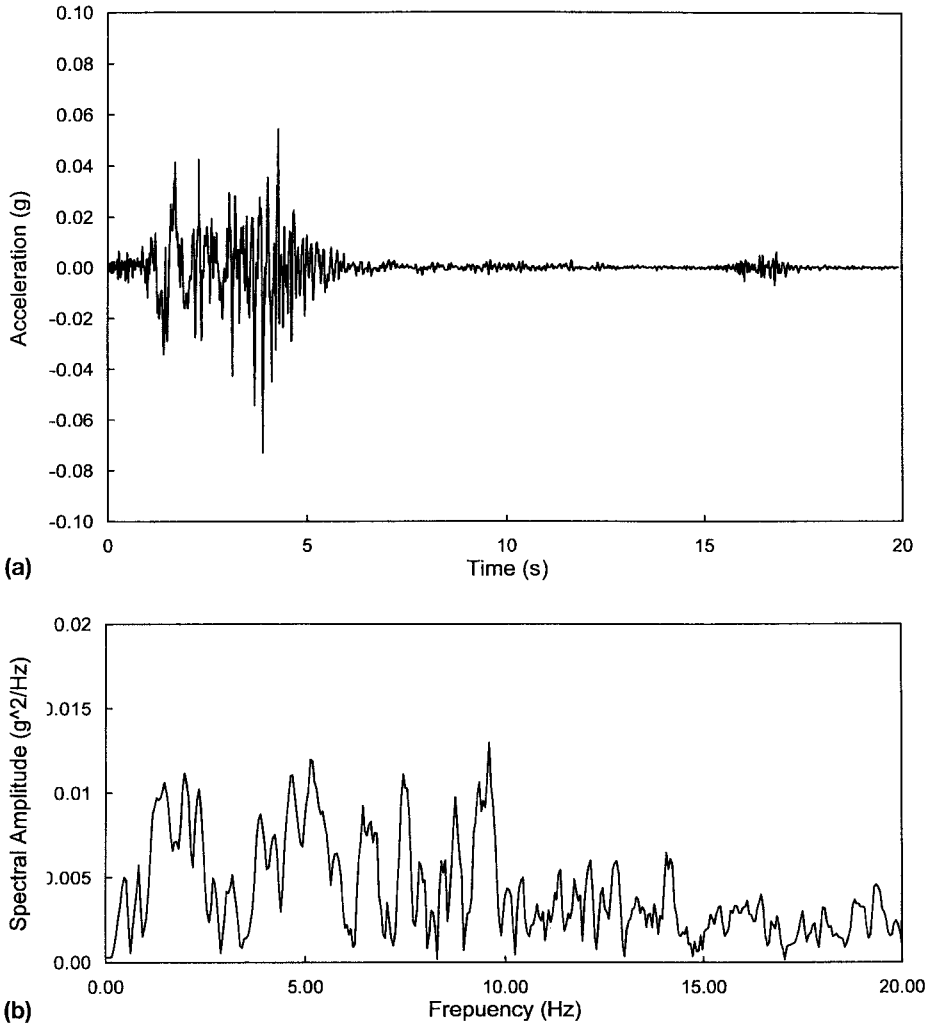

FIG. 11. (a) Time History; (b) Acceleration Spectrum of Base Motion Two

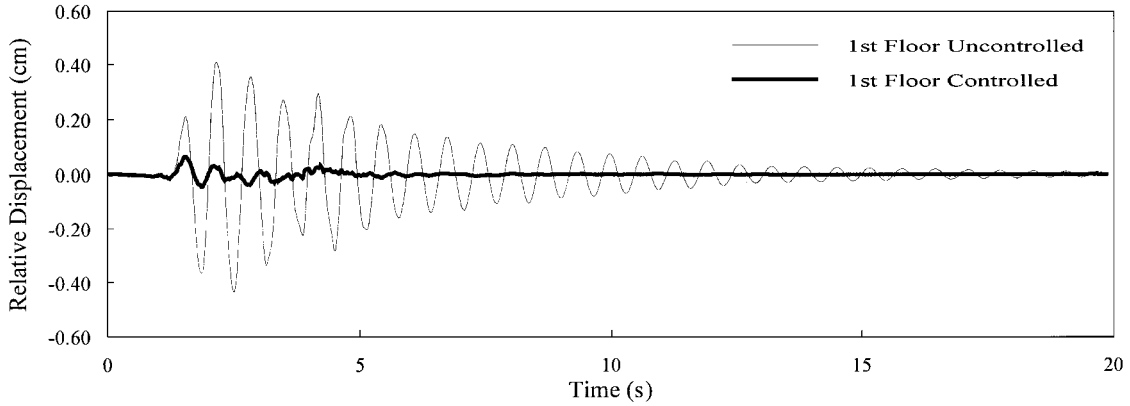

FIG. 12. Controlled and Uncontrolled Relative Displacements of First Floor of Three-Story Structure Subjected to Base Motion Two

Likewise, the control indices are 0.992, 0.915, and 0.860 for the first, second, and third floors of the structure, respectively, subjected to base motion two. Notably, results in this study indicate that the structural responses are significantly reduced for the first and second floors. The third (upper) floor displays less control effectiveness during the former period of the time history, while good control effectiveness is achieved during the later period of the time history. Less control effectiveness on the third floor during the former period of the time history occurs because only one active tendon controller is used and installed on the first floor. We believe that the control effectiveness for the upper floor is improved if the active tendon controller is installed on the third floor.

SUMMARY AND CONCLUSIONS

In this work, we present an active pulse control algorithm. The underlying notion of the active pulse control algorithm largely rests on the physical realization that the accumulation of a series of small responses always causes large structural responses under dynamic loading. In addition, a pulse control force in the active pulse control algorithm aims to eliminate

J. Eng. Mech. 2000.126:839-849.

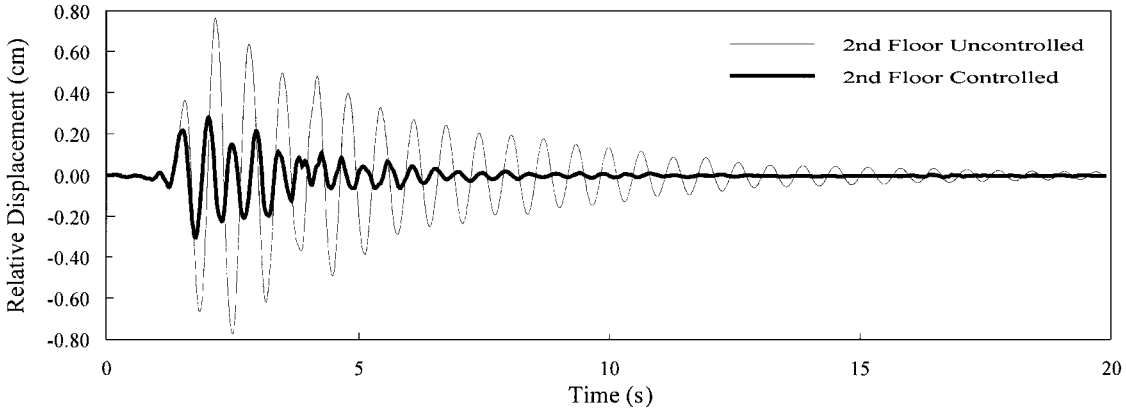

FIG. 13. Controlled and Uncontrolled Relative Displacements of Second Floor of Three-Story Structure Subjected to Base Motion Two

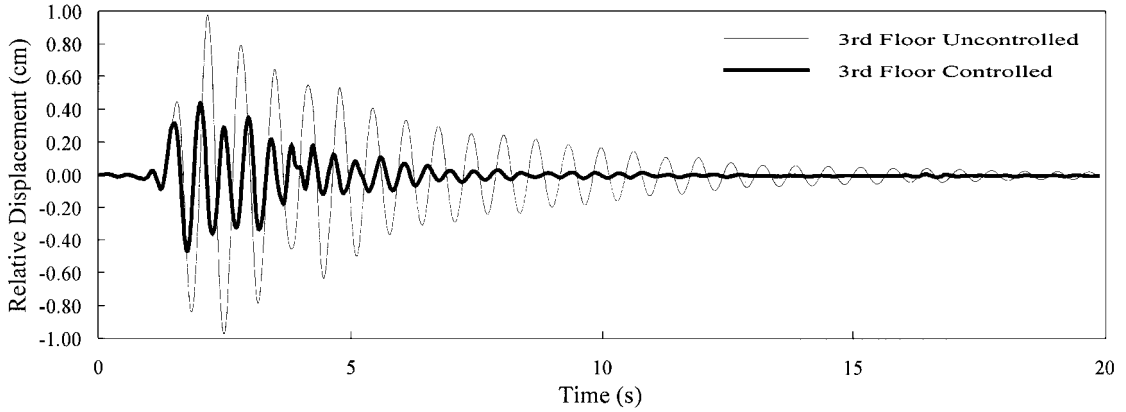

FIG. 14. Controlled and Uncontrolled Relative Displacements of Third Floor of Three-Story Structure Subjected to Base Motion Two

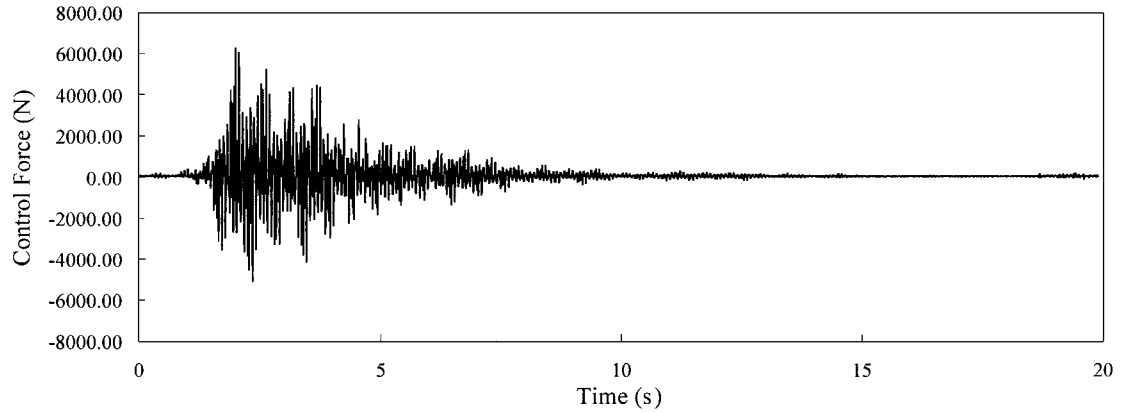

FIG. 15. Time History of Pulse Control Force for Three-Story Structure Subjected to Base Motion Two

the cumulative structural responses. The effect of pulses is postponed to the time that is a small interval before the next sampling time so that the control force can be calculated in time and applied. Therefore, the problem of time delay due to the computation time is circumvented in the proposed control strategy.

For simplicity, assume that only one active tendon controller is used. However, all the relative displacements and relative velocities cannot be kept after controlling each degree of freedom at zero by a single pulse control force. Therefore, minimizing the cumulative structural responses allows us to apply the pulse control force. To reduce or alleviate the limitations of the conventional control algorithm, an ANN model is incorporated into the active pulse control algorithm, referred to herein as the adaptive neural structural active pulse (ANSAP) controller to control civil engineering structures under dynamic loadings. The control strategy of the ANSAP controller aims to minimize the structural cumulative responses during earthquakes by applying the active pulse control force. Analysis of the linear SDOF system reveals that the active control algorithm destroys the gradual rhythmic buildup of the structural response and reduces the structural responses significantly at the peak of the relative displacements. In addition, a three-degree-of-freedom linear system demonstrates the control effectiveness of the ANSAP controller. Notably, the performance of the ANSAP controller trained using the recorded data of the El Centro earthquake is also practical for addressing the Pacoima earthquake, which was never used in training

J. Eng. Mech. 2000.126:839-849.

the ANSAP controller. Although this example shows less control effectiveness on the upper floor, the structural responses are significantly reduced at the later period of the time history. The above issue can be resolved by installing an active tendon controller on the upper floor or installing active tendon controllers on every floor. We believe that the ANSAP controller is also useful when extended to a system with many more degrees of freedom and nonlinear systems.

ACKNOWLEDGMENT

The writers would like to thank the National Science Council of the Republic of China for financially supporting this research under Contract No. NSC 88-2211-E-009-001.

APPENDIX. REFERENCES

Adeli, H., and Hung, S. L. (1995). *Machine learning—Neural networks, genetic algorithms, and fuzzy systems*, Wiley, New York.

Chung, L. L., Reinhorn, A. M., and Soong, T. T. (1988). ''Experiments on active control of seismic structures.'' *J. Engrg. Mech.*, ASCE, 114(2), 241–256.

Housner, G. W., Soong, T. T., and Masri, S. F. (1994). ''Second generation of active structural control in civil engineering, final program and abstracts.'' *1st World Conf. on Struct. Control*, Int. Assoc. for Struct. Control, University of Southern California, Los Angeles.

Hung, S. I., and Lin, Y. L. (1994). ''Application of an L-BFGS neural network learning algorithm in engineering analysis and design.'' *Proc., 2nd Nat. Conf. on Struct. Engrg.*, Chinese Society of Structural Engineering, Nantou, Taiwan, R.O.C., 221–230.

Johan, A. K., Joos, P. L., and Bart, L. R. (1996). *Artificial neural networks for modeling and control of non-linear systems*, Kluwer Academic, Boston.

Masri, S. F., Bekey, G. A., and Caughey, T. K. (1981). ''Optimum pulse control of flexible structures.'' *J. Appl. Mech., Trans.*, ASME, 48, 619–626.

Nikzad, K., and Ghaboussi, J. (1991). ''Application of multi-layered feedforward neural networks in digital vibration control.'' *Proc., Int. Joint Conf. on Neural Networks*, IEEE Service Center, Piscataway, N.J., II A-1004.

Nocedal, J. (1980). ''Updating quasi-Newton matrix with limited storage.'' *Math. Computation*, 35, 20–33.

Pantelides, C. P., and Nelson, P. A. (1995). ''Continuous pulse control of nonlinear structures.'' *Comp. and Struct.*, 55(6), 997–1006.

Reinhorn, A. M., Soong, T. T., Riley, M. A., Lin, R. C., Aizawa, S., and Higashino, M. (1993). ''Full-scale implementation of active control. II: Installation and performance.'' *J. Struct. Engrg.*, ASCE, 119(6), 1935–1960.

Rumelhart, D. E., Hinton, G. E., and Williams, R. J. (1986). ''Learning international representation by error propagation.'' *Parallel distributed processing*, D. E. Rumelhart, et al., eds., MIT Press, Cambridge, Mass., 318–362.

Sage, A. P., and White, C. C. (1977). *Optimum systems control*, Prentice Hall, Englewood Cliffs, N.J.

Soong, T. T. (1990). *Active structural control: Theory and practice*, Longman Scientific and Technical, Essex, N.Y.

Tang, Y. (1995). ''Active control of SDF systems using artificial neural networks.'' *Comp. and Struct.*, 60(5), 695–673.

Udwadia, F. E., and Tabaie, S. (1981a). ''Pulse control of single-degree-of-freedom system.'' *J. Engrg. Mech.*, ASCE, 107(6), 997–1009.

Udwadia, F. E., and Tabaie, S. (1981b). ''Pulse control of structural and mechanical systems.'' *J. Engrg. Mech.*, ASCE, 107(6), 1011–1028.

Wen, Y. K., Ghaboussi, J., Venini, P., and Nikzad, K. (1992). ''Control of structures using neural networks.'' *Proc., US/Italy/Japan Workshop on Struct. Control and Intelligent Syst., USC Publ. No. CE9210*, University of Southern California, Los Angeles, 232–251.

Yang, J. N., Akbarpour, A., and Ghaemmaghami, P. (1987). ''New optimal control algorithm for structural control.'' *J. Engrg. Mech.*, ASCE, 113(9), 1369–1386.

J. Eng. Mech. 2000.126:839-849.